

First Results from MFOSC-P : Low Resolution Optical Spectroscopy of a Sample of M dwarfs within 100 parsecs

A. S. Rajpurohit¹, Vipin Kumar^{1,2}, Mudit K. Srivastava¹, F. Allard³, D. Homeier⁴,
Vaibhav Dixit¹ and Ankita Patel¹

¹*Astronomy & Astrophysics Division, Physical Research Laboratory, Ahmedabad 380009, India*

²*Indian Institute of Technology, Gandhinagar, India*

³*Univ Lyon, Ens de Lyon, Univ Lyon1, CNRS, Centre de Recherche Astrophysique de Lyon UMR5574, F-69007, Lyon, France*

⁴*Zentrum für Astronomie der Universität Heidelberg, Landessternwarte, Königstuhl 12, 69117 Heidelberg, Germany*

Accepted XXX. Received YYY; in original form ZZZ

ABSTRACT

Mt. Abu Faint Object Spectrograph and Camera (MFOSC-P) is an in-house developed instrument for Physical Research Laboratory (PRL) 1.2m telescope at Mt. Abu India, commissioned in February 2019. Here we present the first science results derived from the low resolution spectroscopy program of a sample of M Dwarfs carried out during the commissioning run of MFOSC-P between February-June 2019. M dwarfs carry great significance for exoplanets searches in habitable zone and are among the promising candidates for the observatory’s several ongoing observational campaigns. Determination of their accurate atmospheric properties and fundamental parameters is essential to constrain both their atmospheric and evolutionary models. In this study, we provide a low resolution ($R \sim 500$) spectroscopic catalogue of 80 bright M dwarfs ($J < 10$) and classify them using their optical spectra. We have also performed the spectral synthesis and χ^2 minimisation techniques to determine their fundamental parameters viz. effective temperature and surface gravity by comparing the observed spectra with the most recent BT-Settl synthetic spectra. Spectral type of M dwarfs in our sample ranges from M0 to M5. The derived effective temperature and surface gravity are ranging from 4000 K to 3000 K and 4.5 to 5.5 dex, respectively. In most of the cases, the derived spectral types are in good agreement with previously assigned photometric classification.

Key words: Instrumentation: Spectrograph, Techniques : Spectroscopy, Stars: low-mass – M dwarfs – Stellar atmosphere – fundamental parameters

1 INTRODUCTION

Small aperture (1-2 meter class) telescopes when equipped with suitable instrumentation can broaden and diversify the scope of various science programs that could be done with such facilities. Recent development of Mt. Abu Faint Object Spectrograph and Camera - Pathfinder (MFOSC-P) instrument (Srivastava et al. 2018) for Physical Research Laboratory (PRL) 1.2m Optical-NIR telescope at Mt. Abu, India offers one such opportunity. The instrument has been developed to provide imaging and low resolution spectroscopy ($R \sim 500-2000$) in optical wavelength regime along the line of widely used Faint Object Spectrograph and Camera (FOSC) series of instruments (e.g. EFOSC (Buzzoni et al. 1984), DFOSC (Andersen et al. 1995) etc.) and was commissioned on the telescope in February 2019. Though MFOSC-P has been conceived as a general user facility instrument for vari-

ety of astrophysical science programs, it can also be utilised for dedicated long term observational programs e.g. understanding the Exo-planet host stars properties. In coherence with the growing importance of Exo-planet sciences e.g. their environments, their host star properties and their dependencies, a dedicated Exo-planet program is being carried out using purpose built PARAS spectrograph with resolution $\sim 67,000$ (Chakraborty et al. 2014, 2018a) on the 1.2m PRL telescope. In coming years the program shall be further enhanced with next generation PARAS-2 spectrograph having resolution $\sim 100,000$ (Chakraborty et al. 2018b) on the upcoming 2.5m PRL optical-NIR telescope at the same site. In general, M dwarf candidates are of particular interest to explore planet search in the habitable zone as they offer suitable conditions in solar neighbourhood with shorter orbital periods. Though their high resolution spectroscopy

are indeed useful for detections and characterisation of host star, their intrinsic low luminosities make them difficult targets for such high resolution spectroscopy programs on small aperture telescopes. On the other hand, low resolution spectrographs like MFOSC-P can target fainter objects and provide very useful insights regarding the host star properties. Thus the feasibility of M-Dwarf characterisation program using low resolution spectra from MFOSC-P was taken as a first dedicated science program during the commissioning run of the instrument.

M dwarfs (0.6 to $0.075 M_{\odot}$) are the most dominant stellar component and contribute around 40% of the total stellar mass of the Galaxy (Chabrier 2003). In the recent past, various space-based as well as ground based surveys (e.g. Wide-field Infrared Survey Explorer - WISE (Wright et al. 2010), Sloan Digital Sky Survey - SDSS (York et al. 2000), Two Micron All Sky Survey - 2MASS (Skrutskie et al. 2006) etc.) have been extremely useful to provide the unprecedented photometric and spectroscopic data of cool M dwarfs. Being the suitable targets for various exoplanet search programs, a good number of bright M dwarfs candidates in the solar neighbourhood has been surveyed for their photometry (Lépine & Gaidos 2011) and spectroscopy (Reid et al. 1995; Hawley et al. 1996; Lépine et al. 2013; Frith et al. 2013). Survey such as Palomar/Michigan State University (Palomar-MSU) Nearby-Star Spectroscopic Survey (Reid et al. 1995; Hawley et al. 1996) covers a sample of M dwarfs in both northern and southern sky beyond the 25 pc limit with radial velocities accuracy of ± 10 km/sec. This survey was used to determine spectral types, absolute magnitudes and distances of their targets, to identify chromospherically active M dwarfs with H- α emission and to determine the luminosity function (Reid et al. 1995; Hawley et al. 1996). Palomar-MSU survey was further used by Hawley et al. (1996) and Gizis et al. (2002) to study the relation between chromospheric activity and age among early (M0–M2.5) and mid (M3–M6) dwarfs. Later, Lépine et al. (2013) and Frith et al. (2013) performed the spectroscopic observations of bright M-dwarfs (magnitude $J < 9$ and $K < 9$ respectively) in the northern sky, as selected from the SUPERBLINK proper motion catalog and Position and Proper Motion Extended-L (PPMXL) catalogue. Such survey and programs provided an insight into the age, metallicity and evolution of M-dwarfs along with local star formation history.

Determination of fundamental parameters (e.g. effective temperature, metallicity, surface gravity etc.) and atmospheric properties of M dwarfs from their spectra are also of much significance. However, the atmospheric properties of M dwarfs changes significantly from early M dwarfs to late M dwarfs (M0 to M9). The presence of complex molecular bands (e.g. Titanium oxide (TiO), Vanadium oxide (VO) in the optical and hydrides such as CaH, FeH in the Near-Infrared (NIR) spectra of M dwarfs etc.) make access to M dwarfs true continuum very difficult and cause uncertainties in determination of their atmospheric properties and fundamental parameters. Recently, Rajpurohit et al. (2013, 2014, 2016, 2018b,a) and Passegger et al. (2016, 2019) compared observed optical and NIR spectra of M dwarfs with their synthetic spectra to determine their atmospheric properties and fundamental parameters. Model atmosphere such as BT-Settl which account for recent advancement in various line list by (Plez 1998) and (Barber et al. 2006) along with

dust formation (Allard et al. 2003, 2012, 2013) is now able to reproduce the shape of the spectral energy distribution (SED) down to late M dwarfs (M9) and have improved the previous estimates significantly from earlier studies (Allard & Hauschildt 1995; Rajpurohit et al. 2012).

The principal aim of this paper is to perform the spectroscopic observations to classify and to determine the atmospheric properties and fundamental parameters of a sample of M dwarfs; thereby showing the importance of suitable instrumentation on small aperture telescopes for M Dwarfs studies and usefulness of MFOSC-P for such programs in particular. Our sample of M dwarfs along with observations and data reduction are described in Section 2. Section 3 describes the spectroscopic classification based on the comparison with the template spectra. The determination of fundamental parameters of M dwarfs in our sample is described in Section 4. Section 5 discusses about the H- α emission detected in M dwarfs. In section 6 we have discussed and summarise our results.

2 SPECTROSCOPIC OBSERVATIONS AND DATA REDUCTION

The observations were performed during the commissioning run of MFOSC-P instrument on PRL 1.2m, f/13 Telescope. We had selected bright M-Dwarf sources from the all sky catalog of bright M dwarfs (Lépine & Gaidos 2011), typically with V magnitude brighter than 14 and covering a wide sub-spectral types. A total of 80 suitable targets were observed between February-June 2019. The authors refer to (Lépine & Gaidos 2011) for more detail of the brightest M dwarfs candidates with magnitude $J < 10$. The details of these targets are summarized in Table 1. Parallax for these sources are obtained from GAIA DR-2 archive (Luri et al. 2018) are given as reference. These parallaxes are converted to the distance (pc) as per the method and tool given in Luri et al. (2018). All of these sources are within the distance of 100 pc.

MFOSC-P is a fully in-house developed camera and spectrograph based on the concept of Faint Object Camera and Spectrograph (FOSC) series of instruments. The instrument provides seeing limited imaging with a sampling of 3.3 pixels per arc-seconds over the field of view of 5.2 X 5.2 square arc-minutes. MFOSC-P uses three plane reflection gratings having 500, 300 and 150 line-pairs (lp)/mm to provide slit limited resolutions with dispersion of ~ 1.1 Å per pixel, 1.9 Å per pixel and 3.8 Å per pixels respectively. Two slits of 75 microns and 100 microns width (corresponding to 1.0 and 1.3 arc-seconds on the sky) are provided for varying seeing conditions. For more detail regarding the MFOSC-P instrument, the authors refer to Srivastava et al. (2018). Another paper on the development, commissioning and characterization of the instrument is currently in preparation. The target M-Dwarfs in our sample were observed using 150 lp/mm grating covering the spectral range of 4800-8300 Å with a slit width of 1 arc-second. The sources were observed for integration time in range of 500-1500 seconds per object. Wavelength calibration spectra were recorded immediately after the each of the science spectra in the same settings of the instrument and orientation of telescope. MFOSC-P instrument is equipped with Halogen and spectral calibra-

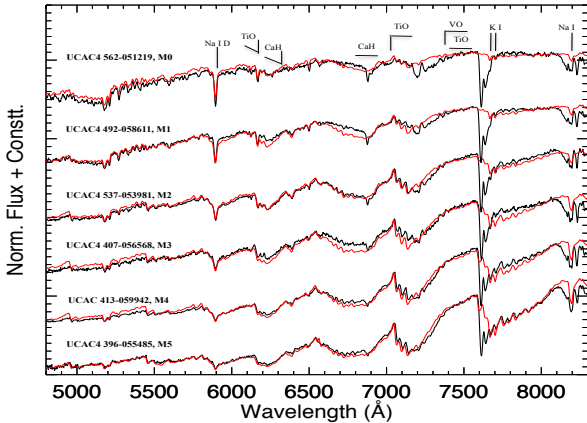


Figure 1. SDSS template spectra (red) taken from [Bochanski et al. \(2007\)](#) is compared with observed spectral sequence of M dwarfs (black). Representative spectra of different subclasses from our sample are chosen to show the match. The most prominent spectral features along with the derived spectral type are also labeled.

tion lamps. Neon and Xenon calibration lamps are used for wavelength calibration. Spectro-photometric standard stars from ESO catalogue¹ were also observed for the instrument response correction.

The raw data were later reduced using self developed data analysis routines in Python using astronomical image processing libraries (e.g. *astropy* etc.) available in public domain. The steps include bias subtraction, cosmic ray removal, tracing and extracting the spectra, sky background subtraction etc. Pixel to pixel response variations were determined using halogen spectra and were found to be less than 1%, thus not applied to the observed spectra. Wavelength solution was determined from the spectral lamps spectra recorded immediately after the science observations. A third order polynomial fit was used to generate pixel versus wavelength relation.

Though second order contamination from blue part is expected to be there at the redder part of the spectrum, the targets like M dwarfs are redder in spectrum and typically have U to I band flux ratio of nearly 1:100. Thus, given the spectral throughput of the instrument along with the telescope in blue part, blaze function of the grating and spectral energy distribution (SED) of the objects second order spectral contamination are minimal. Nevertheless, even though the observed spectral range are up to 8300 Å, we have restricted our analysis within the wavelength range of 4800-8100 Å (see sections 3 and 4).

3 FOLLOW-UP SPECTROSCOPIC CLASSIFICATION

Over the last few decades, several schemes have been proposed for M dwarfs classification. These schemes, mostly

based on spectral shape and features of the M dwarf spectra, are used to preliminary classify them according to their fundamental parameters and atmospheric properties.

The spectral energy distribution (SED) and the broadband colours of M dwarfs are mostly governed by the various molecular opacities e.g. TiO, VO and hydrides bands etc both in the optical and in the NIR. The strength of these opacities varies from early type M dwarf (M0 type) to late type (M5 or later) for example, the broad molecular bands such as from TiO are stronger in early M dwarfs while VO and hydrides (CaH) bands are stronger ([Allard et al. 2000](#)) in later M dwarfs. The strength of these molecular bands depends on the atmospheric properties and various stellar parameters such as effective temperature (T_{eff}), surface gravity ($\log g$) and metallicity ($[M/H]$) of the M dwarf. Considering such variation in the M dwarf spectra, [Kirkpatrick et al. \(1991\)](#) used the least-squares minimisation technique to classify M dwarfs by comparing the template M dwarf spectra with the target spectrum. Later on [Henry et al. \(2002\)](#) and [Scholz et al. \(2005\)](#) have used a similar technique that compares the low resolution template spectra of M dwarfs with that of the observed M dwarfs spectrum.

[Reid et al. \(1995\)](#) adopted the classification scheme which was based on measuring of the strength of the most prominent molecular bands called "band indices" such as TiO and CaH. Here the ratio of flux between various bandheads to that of the flux in nearby pseudo-continuum was determined which was then used to classify early M dwarfs to mid M dwarfs (M0 to M5). These bands get saturated in late M dwarfs (later than M5), thus VO bandheads were used for the classification ([Kirkpatrick et al. 1995](#)). [Martín et al. \(1999\)](#) assigns the spectral type to late M dwarfs based on the pseudo-continuum spectral ratios (namely PC3). [Gizis \(1997\)](#) further classified them in to the sub category of M subdwarfs based on the strength and ratio of CaH and TiO molecular bandheads. This work was later expanded by [Lépine et al. \(2003\)](#) and [Lépine et al. \(2007\)](#).

While the above works utilise the high resolution spectra, [Scholz et al. \(2005\)](#) shows that the comparison of low resolution spectral template provides an accurate classification of M dwarfs. In this work we have utilized the low resolution spectra of M dwarfs covering the spectral regime 4800-8100 Å for their classification. The template spectra of low-mass M dwarfs are taken from [Bochanski et al. \(2007\)](#) to be used as template spectra of such stars from M0 to L0. These template spectra were derived from 4000 SDSS spectra. Similar to the works of ([Kirkpatrick et al. 1995](#)), [Scholz et al. \(2005\)](#) we have adopted the least square minimisation techniques to determine the spectral type of the observed M dwarfs in our sample.

Here we first normalised both the template and observed spectra of M dwarfs. The higher resolution ($R \sim 1800$) SDSS template spectra were then convolved using gaussian kernel at the same resolution as that of the observed spectrum ($R \sim 500$). Later this flux normalised spectra were compared with the template ones for the least square minimisation process to obtain the nearest match. The spectral type of this nearest match was then assigned to the observed M dwarf (Table 2). We expect the error to be of one spectral class in this method as the template spectra themselves are at the spacing of one spectral class.

¹ <https://www.eso.org/sci/observing/tools/standards/spectra/stanlis.html> Figure 1 shows the comparison of a set of observed spec-

Table 1. Properties of M dwarfs sample used in this study along with their coordinates. Optical and Near-infrared photometry is compiled from [Ochsenbein et al. \(2000\)](#) and [Lépine & Gaidos \(2011\)](#). The parallaxes of M dwarfs in our sample is taken from GAIA DR-2 database ([Luri et al. 2018](#)).

Source Name	RA	Dec	V (mag)	R (mag)	I (mag)	J (mag)	H (mag)	K (mag)	GAIA parallax (mas)	Distance (parsec)
Css833	13h48m34.02s	+31d59m56.89s	12.34	11.91	-	9.02	8.43	8.22	34.083	29.34
G123-74	12h57m32.41s	+40d57m00.89s	13.23	12.43	10.20	9.22	8.57	8.38	24.400	40.98
G138-64	16h46m13.76s	+16d28m41.08s	11.65	10.60	9.27	7.95	7.29	7.09	63.407	15.77
G138-7	16h11m28.10s	+07d03m59.98s	14.08	13.41	10.60	9.77	9.28	9.02	36.411	27.46
G177-8	12h58m17.17s	+52d36m43.70s	13.19	12.40	10.40	9.29	8.72	8.50	38.105	26.24
G19-12	17h04m49.57s	+01d30m35.47s	13.47	12.92	10.90	9.60	8.97	8.75	-	-
GJ3584	10h04m32.76s	+05d33m41.25s	12.67	12.22	9.90	9.02	8.40	8.18	-	-
GJ3696	11h58m17.61s	+42d34m28.96s	14.43	13.76	10.60	9.59	8.98	8.71	46.028	21.73
GJ3697	11h58m59.45s	+42d39m39.81s	12.09	11.65	9.90	8.64	8.05	7.82	-	-
GJ3763	13h08m50.52s	+16d22m03.58s	13.48	12.71	10.20	9.26	8.65	8.41	35.918	27.84
GJ3793	13h34m49.35s	+20d11m38.67s	14.25	13.42	10.80	9.67	9.10	8.85	18.232	54.85
GJ3822	14h02m19.62s	+13d41m22.76s	10.64	9.69	8.68	7.56	6.89	6.71	49.175	20.34
GJ3873	14h54m27.92s	+35d32m56.94s	12.55	12.13	9.50	8.24	7.71	7.47	67.072	14.91
GJ3895	15h11m55.96s	+17d57m16.42s	13.98	12.90	10.60	9.56	9.06	8.77	41.228	24.26
LP324-7	13h51m45.13s	+31d42m57.67s	13.40	12.46	10.60	9.59	8.93	8.75	14.402	69.44
LP324-72	14h08m10.47s	+28d11m13.93s	12.75	12.31	10.60	9.73	9.06	8.90	19.749	50.64
LP378-897	13h16m40.56s	+23d15m42.43s	13.51	13.03	10.70	9.76	9.11	8.85	27.695	36.11
LP435-110	12h26m38.10s	+17d28m11.14s	13.63	12.74	10.50	9.64	9.01	8.79	25.938	38.55
LP671-33	10h46m07.05s	-08d22m14.77s	12.74	12.32	11.00	9.86	9.21	9.03	17.702	56.49
LP738-44	13h37m30.00s	-10d48m34.92s	12.46	12.10	-	9.73	9.09	8.91	-	-
StKM1-1125	14h08m40.58s	+23d50m54.94s	12.34	11.86	10.20	9.29	8.62	8.40	20.267	49.34
StKM1-1077	13h35m16.12s	+30d10m56.67s	11.67	11.30	-	8.76	8.14	7.91	25.689	38.93
StM186	13h41m27.65s	+48d54m45.87s	12.98	12.62	10.20	9.00	8.45	8.19	-	-
TYC2009-522-1	14h04m10.24s	+26d26m24.02s	12.33	11.92	-	9.83	9.21	9.03	14.545	68.75
UCAC3 160-122037	13h16m49.39s	-10d19m18.27s	13.92	13.71	11.29	9.97	9.43	9.11	-	10.00
UCAC4 396-055485	13h21m56.31s	-10d52m09.88s	13.90	13.70	11.00	9.52	8.82	8.62	18.818	53.14
UCAC4 407-056568	13h26m56.92s	-08d45m47.01s	12.99	12.58	-	9.45	8.86	8.59	-	-
UCAC4 407-057475	13h55m12.70s	-08d42m25.93s	13.00	12.80	-	9.25	8.65	8.40	28.976	34.51
UCAC4 421-056421	12h06m07.44s	-05d50m01.88s	13.16	12.77	-	9.97	9.33	9.06	18.425	54.27
UCAC4 436-076101	18h25m48.64s	-02d58m17.15s	13.05	12.64	-	9.62	8.95	8.75	21.076	47.45
UCAC4 448-055886	13h26m26.40s	-00d26m52.86s	12.48	12.07	-	9.89	9.28	9.08	13.105	76.31
UCAC4 450-057508	15h09m50.64s	-00d07m51.77s	12.33	11.91	-	9.51	8.90	8.69	19.318	51.77
UCAC4 451-054724	13h27m06.68s	+00d00m48.29s	13.02	12.57	-	9.74	9.13	8.91	23.360	42.81
UCAC4 451-055381	13h51m13.78s	+00d04m26.98s	13.06	12.82	-	9.90	9.25	9.04	18.456	54.18
UCAC4 451-081123	18h27m41.08s	+00d11m15.07s	12.92	12.65	-	9.48	8.89	8.60	-	-
UCAC4 467-056893	16h50m11.00s	+03d14m40.08s	14.03	13.30	-	9.72	9.19	8.92	-	-
UCAC4 484-057552	15h29m48.62s	+06d38m16.52s	12.69	12.23	-	9.99	9.34	9.16	10.529	94.97
UCAC4 496-060421	13h37m17.62s	+09d08m00.56s	12.86	12.48	-	9.34	8.77	8.50	27.347	36.57
UCAC4 528-054911	12h44m24.96s	+15d32m12.49s	13.86	13.45	-	9.99	9.40	9.16	23.280	42.96
UCAC4 534-051996	11h52m20.53s	+16d40m19.14s	13.54	13.16	-	9.73	9.17	8.92	34.955	28.61
UCAC4 540-054017	13h27m30.59s	+17d48m08.31s	12.66	12.27	-	9.83	9.18	9.01	15.333	65.22
UCAC4 546-052448	13h54m10.86s	+19d01m16.66s	13.50	13.27	-	9.59	8.94	8.69	31.123	32.13
UCAC4 548-070636	18h20m35.82s	+19d27m55.67s	12.81	12.21	10.30	9.57	8.88	8.70	17.700	56.50
UCAC4 550-052262	13h15m49.21s	+19d57m07.95s	13.58	13.15	-	9.87	9.25	8.99	28.602	34.96
UCAC4 570-051422	14h08m40.58s	+23d50m54.94s	12.34	11.86	10.20	9.29	8.62	8.40	20.267	49.34
UCAC4 570-051538	14h14m35.09s	+23d57m24.84s	12.53	12.39	10.70	9.78	9.13	8.98	13.737	72.80
UCAC4 574-047909	12h35m33.43s	+24d39m18.44s	13.43	13.05	10.80	9.93	9.25	9.06	13.174	75.91
UCAC4 587-051209	15h11m04.82s	+27d12m44.71s	13.13	12.58	10.60	9.53	8.93	8.70	24.985	40.02
UCAC4 599-049146	11h59m13.54s	+29d36m09.07s	13.26	12.64	-	9.89	9.34	9.11	-	-
UCAC4 605-050828	14h04m08.56s	+30d49m34.50s	13.03	12.54	-	9.43	8.76	8.52	26.001	38.46
UCAC4 607-049137	14h10m15.46s	+31d15m36.55s	13.86	13.26	-	9.96	9.30	9.03	-	-
UCAC4 615-064218	18h44m20.37s	+32d50m46.33s	13.73	13.06	-	9.65	9.05	8.80	29.039	34.44
UCAC4 629-047283	13h25m55.16s	+35d46m42.88s	13.48	12.82	10.40	9.64	9.09	8.84	29.349	34.07
UCAC4 630-046962	11h52m57.15s	+35d54m45.91s	13.69	13.41	11.20	9.96	9.35	9.13	25.112	39.82
UCAC4 640-048822	14h07m07.51s	+37d52m22.99s	12.57	12.17	10.50	9.67	9.02	8.83	17.232	58.03
UCAC4 641-058022	18h06m17.74s	+38d01m49.79s	12.23	11.55	10.20	9.32	8.66	8.48	8.670	115.34
UCAC4 647-050041	12h54m29.25s	+39d19m56.78s	13.32	12.89	10.70	9.97	9.35	9.13	19.221	52.03
UCAC4 687-054755	13h25m18.24s	+47d20m37.32s	12.68	12.16	10.50	9.74	9.12	8.89	17.925	55.79
UCAC4 719-054147	15h25m48.82s	+53d44m16.30s	12.70	12.26	-	9.86	9.21	9.02	17.079	58.55
UCAC4 724-051511	13h27m01.69s	+54d36m13.77s	12.88	12.61	10.90	9.87	9.27	9.04	19.643	50.91
UCAC4 731-051425	13h17m23.17s	+56d10m13.50s	13.38	13.09	10.80	9.80	9.22	8.98	26.768	37.36
UCAC4 780-025091	13h11m59.55s	+65d50m01.79s	12.95	12.58	10.60	9.71	9.06	8.84	27.740	36.05
UCAC4 413-059942	14h16m33.28s	-07d25m38.24s	13.76	13.47	-	9.81	9.20	8.94	17.242	58.00
UCAC4 413-060157	14h23m01.24s	-07d34m01.11s	13.20	12.92	10.38	9.59	8.99	8.73	31.004	32.25
UCAC4 457-046840	10h06m21.82s	+01d21m23.18s	13.77	13.57	-	9.53	9.00	8.70	39.547	25.29
UCAC4 462-046617	10h35m46.92s	+02d15m58.21s	13.57	13.23	-	9.83	9.22	8.97	-	-
UCAC4 492-058611	13h49m07.33s	+08d23m36.09s	12.18	11.67	-	9.34	8.76	8.55	17.878	55.94
UCAC4 518-059332	15h47m11.96s	+13d34m40.78s	13.15	12.78	-	9.89	9.20	9.03	-	-
UCAC4 529-059437	16h27m46.42s	+15d42m06.13s	13.16	12.70	11.10	9.98	9.38	9.17	20.594	48.56
UCAC4 536-067333	17h44m12.95s	+17d06m12.14s	13.32	12.81	10.80	9.94	9.32	9.11	19.410	51.52
UCAC4 537-053981	13h35m12.46s	+17d14m08.88s	13.19	12.73	10.80	9.87	9.21	9.03	13.898	71.95
UCAC4 544-056450	15h51m39.13s	+18d40m23.54s	13.05	12.53	10.60	9.80	9.11	8.90	20.595	48.56
UCAC4 547-049435	11h05m19.44s	+19d18m34.24s	13.82	13.35	-	9.87	9.28	9.01	23.696	42.20
UCAC4 562-051219	12h23m43.46s	+22d15m17.08s	12.36	11.95	10.50	9.89	9.31	9.14	10.281	97.27
UCAC4 562-057449	16h38m25.33s	+22d22m41.54s	13.06	12.54	10.80	9.61	9.05	8.82	30.562	32.72
UCAC4 598-053572	15h39m05.72s	+29d31m40.62s	13.11	12.65	-	9.76	9.18	8.94	23.604	42.37
UCAC4 629-050950	16h27m37.57s	+35d41m42.94s	13.71	13.31	10.60	9.60	9.02	8.74	35.924	27.84
UCAC4 647-048900	11h31m16.41s	+39d23m02.91s	13.05	12.64	10.60	9.70	9.12	8.88	27.390	36.51
UCAC4 682-053954	14h13m46.76s	+46d18m22.73s	13.14	12.64	10.40	9.43	8.80	8.59	25.434	39.32
UCAC4 507-054072	13h15m47.39s	+11d16m25.77s	13.20	12.77	-	9.76	9.16	8.95	19.186	52.12

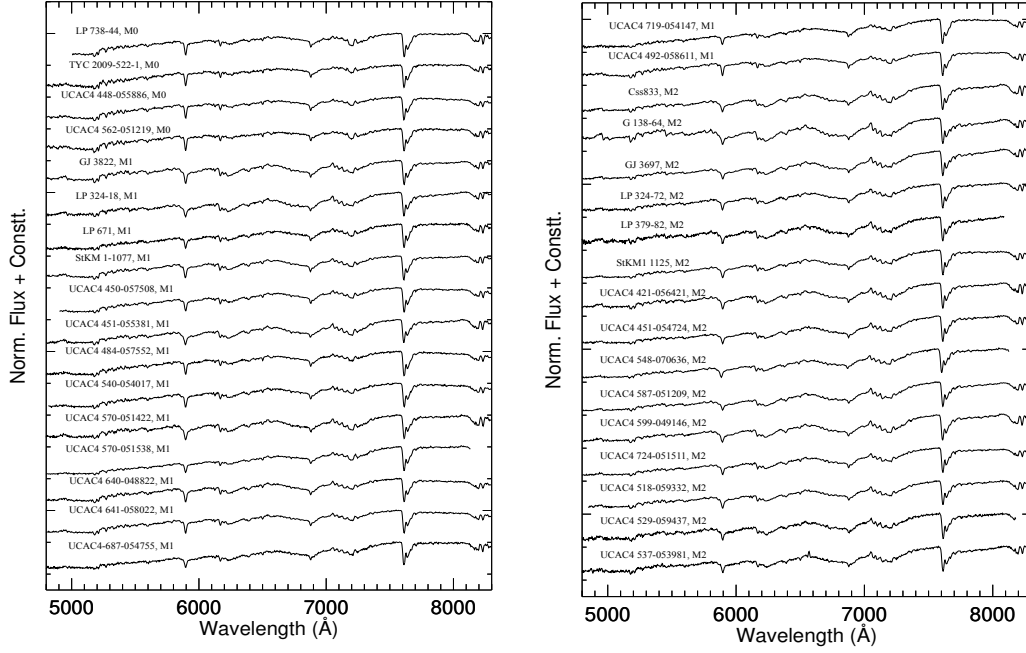


Figure 2. Optical spectra of *M* dwarfs from spectral sequence M0 to M2 observed with the MFOSC.

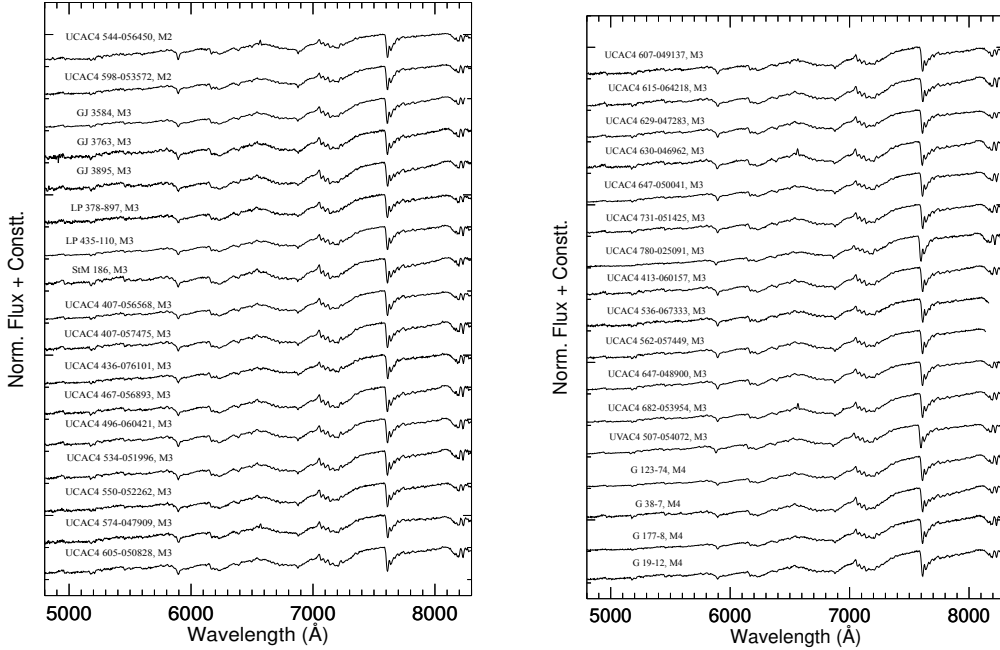


Figure 3. Same as fig. 2 but for spectral sequence from M2 to M4.

tral sequence of *M* dwarfs in our sample with the SDSS standard *M* dwarfs template spectra along with the most prominent spectral features. We also tried to classify the *M* dwarfs in our sample by calculating spectral indices method developed by Reid et al. (1995) using the band strengths of TiO and CaH. However, the resolution of our spectra was not good enough to achieve reliable spectral types. Figure 2, 3, and 4 shows the observed spectra of *M* dwarfs in our sample along with their spectral type derived from the

method describe above. Most of the sources shows similar spectral sub classification or within one class of their photometric classification Lépine & Gaidos (2011). In four cases the difference is two or three subclasses.

4 FUNDAMENTAL PARAMETERS

Fundamental stellar parameters of our sample targets were determined by comparing the observed spectra with the

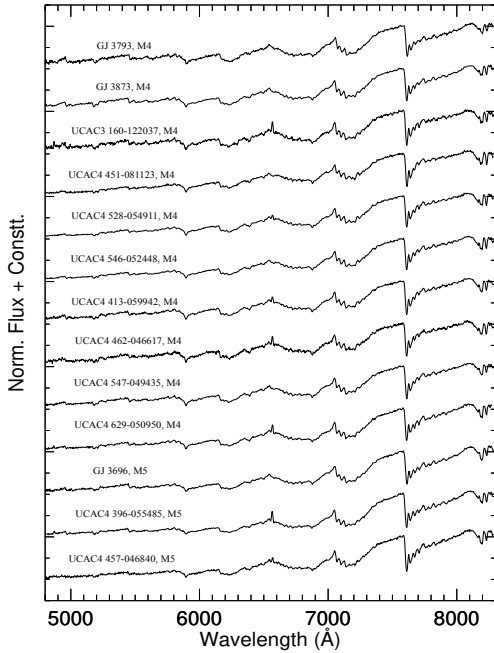


Figure 4. Same as fig. 2 but for spectral sequence from M4 to M5.

synthetic spectra generated by the BT-Settl version of PHOENIX (Allard et al. 2010, 2011, 2013). The BT-Settl model grid spans the T_{eff} between 300 and 7000 K in the steps of 100 K, $\log g$ ranges from 2.5 to 5.5 at a step of 0.5 dex and metallicity $[M/H]$ ranges from -2.5 to +0.5 at a step of 0.5 dex. These models account for the latest solar abundances by Caffau et al. (2009, 2011) with updated water vapour opacities (Barber & Tennyson 2008). Various microphysical process as well as dust and cloud formation along with the gravitational settling (Allard et al. 2012) has also been included in these models. Recently, Rajpurohit et al. (2012, 2013, 2014, 2018a,b) have validated the BT-Settl models by comparing the low resolution ($\Delta\lambda = 10 \text{ \AA}$) as well as the high resolution ($R = 20,000$ and $90,000$) optical and near-infrared spectra (NIR) with the BT-Settl models in the grid range of $2400 \leq T_{\text{eff}} \leq 4000 \text{ K}$.

The BT-Settl model grid used in this study for the comparison spans T_{eff} between 3000 to 4000 K in steps of 100 K and $\log g$ ranges from 4.0 to 5.5 in steps of 0.5 dex. Since M dwarfs in our sample lies within 100 pc of the solar neighbourhood and belongs to the disc population (Lépine & Gaidos 2011), so we do not expect large deviations from solar metallicity. Thus we have used the models with the solar metallicity ($[M/H] = 0.0$) for the comparison. The comparison of BT-Settl synthetic spectra with the observed spectra involves the process of degrading the high resolution synthetic spectra at a resolution of the observed spectra by using a Gaussian convolution. We then employed the χ^2 method as discussed in Rajpurohit et al. (2013) to determine the T_{eff} and $\log g$ of M dwarfs in our sample. The spectral range between 5500 to 8100 \AA have been used for the χ^2 calculation. The spectral regions below 5500 \AA (due to low SNR) and between 7600 to 7700 \AA (which includes the telluric absorption) have not been considered in the χ^2 cal-

culations. During the χ^2 calculations, we have not applied any weights on any spectral region for the determination of T_{eff} and $\log g$. We have retained the models that give the lowest χ^2 as the best fit parameters. The best fit models have also been inspected visually by comparing them with the observed spectra. With the given resolution of the observed spectra the error in the derived fundamental parameters are equal the grid spacing of the synthetic spectrum which is 100 K for T_{eff} and 0.5 dex for $\log g$. More details about the procedure of determination of the stellar parameters of M dwarfs, can be found in Rajpurohit et al. (2013). The BT-Settl model is able to reproduce the shape of SED and the profiles of the strong atomic lines such as Na I D, though no attempt has been made to fit the individual atomic lines, such as the K I and Na I resonance doublets. Figure 5, 6, 7 shows the comparison of the entire spectral sequence of M dwarfs (black) with the synthetic spectra (red). The best fit parameters of M dwarfs in our sample is given in Table 2. We have compared T_{eff} and spectral type determined for the individual stars in this study with Rajpurohit et al. (2013) and found a very good agreement between them (Figure 8).

5 CHROMOSPHERIC ACTIVITY

With a thick convection zone above a radiative interior, the low mass stars in particular M dwarfs show a high level of photospheric, chromospheric, and coronal magnetic activities. In this reference, H- α emission at 6563 \AA is of particular importance as this is an indicator of the chromospheric activity in the spectra of M dwarfs (Hawley et al. 1996; Gizis et al. 2002; Reiners & Basri 2008). Hawley et al. (1996) found that late type M dwarfs i.e later than $> M5$ shows that incidence of activity increases monotonically as compared to early M dwarfs. They also showed that the TiO band structure depends on the chromospheric activity level of the star and thus is very useful to constrain the atmospheric model of M dwarfs. Detailed studies of such activities in field M dwarfs and M dwarfs in open clusters is of much importance as they can be used to calibrate their age activity relationship, to determine local star formation history and to understand the substellar mass function (Gizis et al. 2002).

In our sample of 80 M dwarfs, we have detected H- α in 10 of them which is listed in table 2. We will be performing the follow-up spectroscopic study of the variability of the H- α of these objects as well as other active M dwarfs in the literature, as a proxy for the magnetic variability using MFOC-P. Such follow-up study of these objects allow us to understand and correlate various properties such as age or rotation velocity as suggested by Hawley et al. (1996) and Gizis et al. (2002).

6 CONCLUSION

We have performed low resolution spectroscopic follow-up observations of 80 bright M dwarfs. All the 80 M dwarfs used in this study is having $J < 10$ magnitude and are identified from the all-sky catalogue of M dwarfs (Lépine & Gaidos 2011). We have spectroscopically classified all the M dwarfs in our sample by comparing them with the standard SDDS

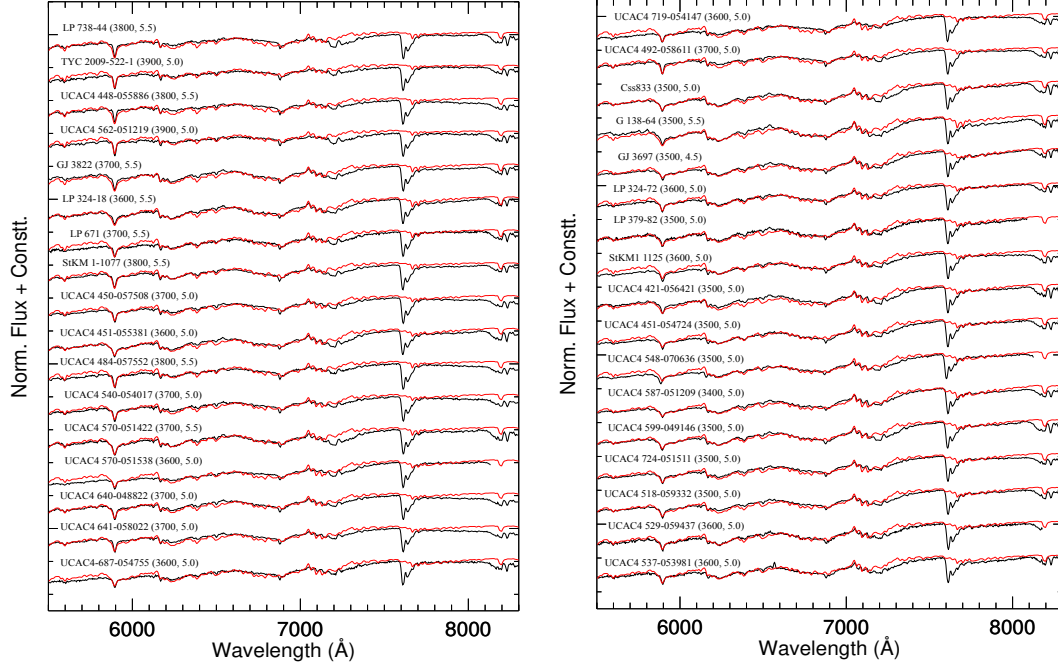


Figure 5. Comparison of observed spectra of M dwarfs (black) ranges from M0 to M2, with the best fit BT-Settl synthetic spectra (red). The model displayed here have $\log g$ ranges from 4.5 to 5.5 and T_{eff} ranges from 3800 K to 3400 K. Telluric features near 7600 to 7700 Å were ignored from the chi-square.

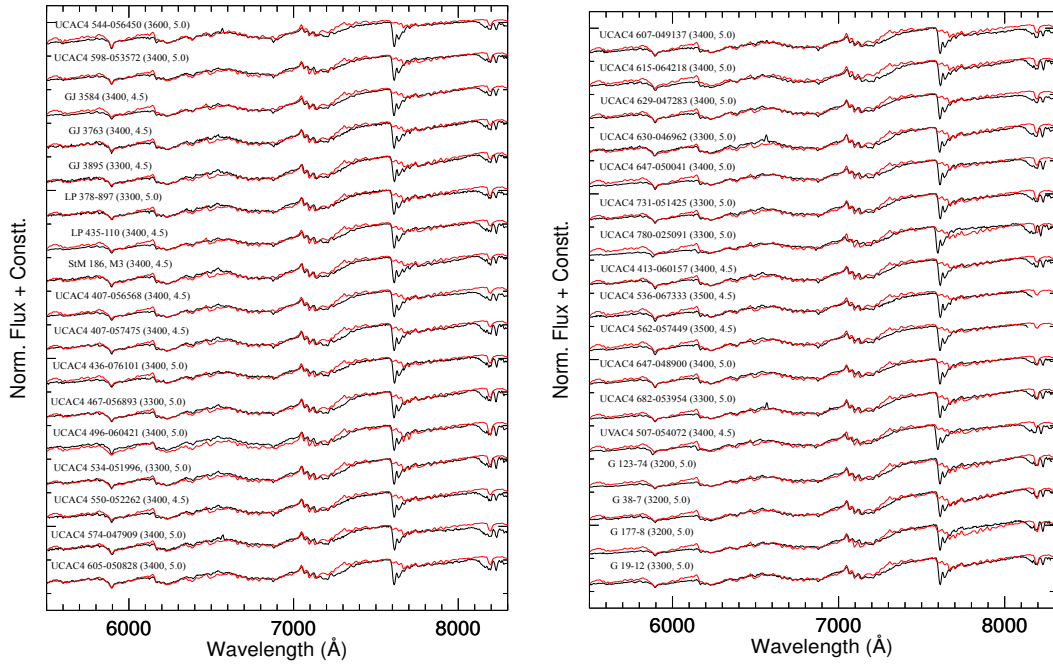


Figure 6. Same as fig. 5 but for spectral type ranges from M2-M4. The model displayed here have $\log g$ ranges from 4.5 to 5.5 and T_{eff} ranges from 3600 K to 3300 K.

template spectra of M dwarfs and assigned spectral type to them. The spectral type of M dwarfs in our sample are ranging from M0 to M5.

We have used the most recent BT-Settl synthetic spectra (Allard et al. 2013) to perform the spectral synthesis analysis and determined their atmospheric parameters, in particular T_{eff} and $\log g$ within an uncertainty of 100 K in

T_{eff} and 0.5 dex in $\log g$. Our T_{eff} of M dwarfs ranges from 4000 K to 3000 K and $\log g$ ranges from 4.5 to 5.5 dex and is extended down to M dwarfs with spectral type M5. The recent BT-Settl model which accounts for the revised solar abundances and TiO line list is able to reproduce the SED of the M dwarfs of entire spectral sequence.

The search for habitable planets around M dwarfs is one

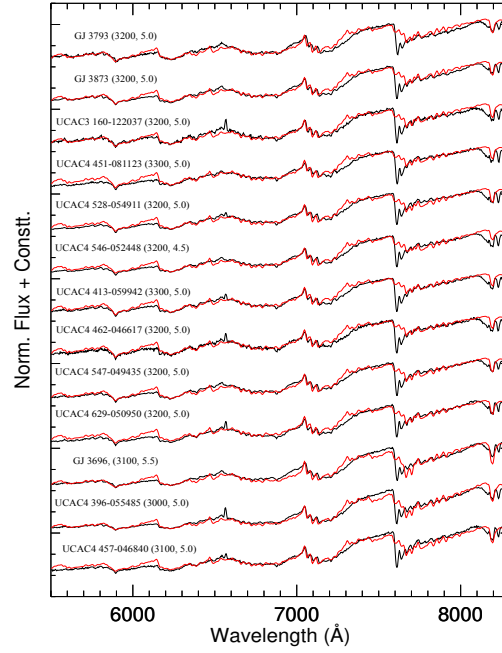


Figure 7. Same as fig. 5 but for spectral type ranges from M4-M5. The model displayed here have $\log g$ ranges from 4.5 to 5.5 and T_{eff} ranges from 3300 K to 3000 K.

Table 2. Stellar parameters of M dwarfs sample determined in this study.

Source Name	Photometric Spectral Type (Lépine & Gaidos 2011)	Derived Spectral Type (This study)	T_{eff} (K)	$\log g$ (cm/sec ²)	Source Name	Photometric Spectral Type (Lépine & Gaidos 2011)	Derived Spectral Type (This study)	T_{eff} (K)	$\log g$ (cm/sec ²)
Css833	M2	M2	3500	5	UCAC4 540-054017	M0	M1	3700	5
G123-74	M3	M2	3500	5.5	UCAC4 546-052448	M4	M4	3200	4.5
G138-64	M3	M4	3200	5	UCAC4 548-070636	M2	M2	3500	5
G138-7	M4	M4	3200	5	UCAC4 550-052262	M3	M3	3400	4.5
G177-8	M3	M4	3200	5	UCAC4 570-051422	M1	M1	3700	5.5
G19-12	M3	M4	3300	5	UCAC4 570-051538	M1	M1	3600	5
GJ3584	M3	M3	3400	4.5	UCAC4 574-047909*	M3	M3	3400	5
GJ3696	M5	M5	3100	5.5	UCAC4 587-051209	M2	M2	3400	5
GJ3697	M2	M2	3500	4.5	UCAC4 599-049146	M2	M2	3500	5
GJ3763	M4	M3	3400	4.5	UCAC4 605-050828	M3	M3	3400	5
GJ3793	M4	M4	3200	5	UCAC4 607-049137	M3	M3	3400	5
GJ3822	M0	M1	3700	5.5	UCAC4 615-064218	M3	M3	3300	5
GJ3873	M4	M4	3200	5	UCAC4 629-047283	M3	M3	3400	5
GJ3895	M4	M3	3300	4.5	UCAC4 630-046962*	M3	M3	3300	5
LP324-18	M3	M1	3600	5.5	UCAC4 640-048822	M1	M1	3700	5
LP324-72	M0	M2	3600	5	UCAC4 641-058022	M0	M1	3700	5
LP378-897	M4	M3	3300	5	UCAC4 647-050041	M2	M3	3400	5
LP435-110	M3	M3	3400	4.5	UCAC4 687-054755	M1	M1	3600	5
LP671-33	M0	M1	3700	5.5	UCAC4 719-054147	M1	M1	3600	5
LP738-44	M0	M0	3800	5.5	UCAC4 724-051511	M2	M2	3500	5
StKM1-1125	M1	M2	3600	5	UCAC4 731-051425	M4	M3	3300	5
StKM1-1077	M0	M1	3800	5.5	UCAC4 780-025091	M2	M3	3300	5
StM186	M4	M3	3400	4.5	UCAC4 413-059942*	M4	M4	3300	5
TYC2009-522-1	M0	M0	3900	5	UCAC4 413-060157	M1	M3	3400	4.5
UCAC3 160-122037*	M4	M4	3200	5	UCAC4 457-046840	M4	M5	3100	5
UCAC4 396-055485*	M4	M5	3000	5	UCAC4 462-046617*	M3	M4	3300	5
UCAC4 407-056568	M3	M3	3400	4.5	UCAC4 492-058611	M0	M1	3700	5
UCAC4 407-057475	M3	M3	3400	4.5	UCAC4 518-059332	M3	M2	3500	5
UCAC4 421-056421	M3	M2	3600	5	UCAC4 529-059437	M3	M2	3600	5
UCAC4 436-076101	M2	M3	3400	5	UCAC4 536-067333	M3	M3	3500	4.5
UCAC4 448-055886	M1	M0	3800	5.5	UCAC4 537-053981*	M3	M2	3600	5
UCAC4 450-057508	M0	M1	3700	5	UCAC4 544-056450*	M2	M2	3600	5
UCAC4 451-054724	M2	M2	3500	5	UCAC4 547-049435	M4	M4	3200	5
UCAC4 451-055381	M2	M1	3600	5	UCAC4 562-051219	M0	M0	3900	5
UCAC4 451-081123	M3	M4	3300	5	UCAC4 562-057449	M3	M3	3500	4.5
UCAC4 467-056893	M4	M3	3300	5	UCAC4 598-053572	M3	M2	3400	5
UCAC4 484-057552	M1	M1	3800	5.5	UCAC4 629-050950*	M4	M4	3200	5
UCAC4 496-060421	M0	M3	3400	5	UCAC4 647-048900	M2	M3	3400	5
UCAC4 528-054911	M4	M4	3200	5	UCAC4 682-053954*	M3	M3	3300	5
UCAC4 534-051996	M4	M3	3300	5	UCAC4 507-054072	M3	M3	3400	4.5

* H- α emission at 6563 Å is detected.

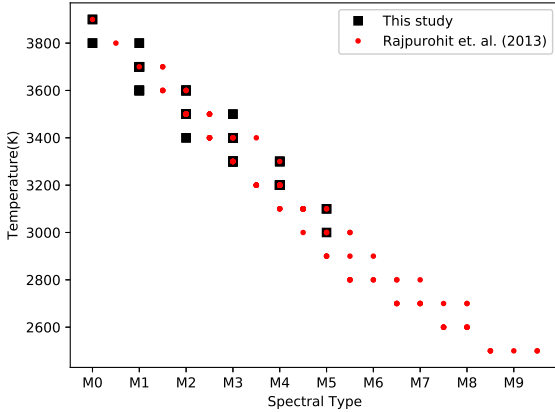


Figure 8. Comparison of T_{eff} versus spectral type relation from this study (black filled square) with that of Rajpurohit et al. (2013) (filled red circles) .

of the most exciting observations programs of recent times. Though in the past such programs were limited by the fewer high resolution spectroscopy facilities and faint nature of such objects, various dedicated upcoming facilities (e.g. high precision radial velocity spectrographs on larger telescopes) are expected to give a big boost to these observations programs. Such methods of high resolution spectroscopy would not only help in the detection of newer planets but also in the studies of planets and host stars environments. While the role of high resolutions spectrum is of great significance, a good deal of information about these objects can still be derived using low resolution spectra on small aperture telescopes. In this work we have attempted one such study for M dwarfs. The spectroscopic catalog presented here, along with their spectral types and stellar parameters, is expected to provide useful list of targets for such surveys. Detection of H- α emission in some of the targets here presents a case to study active M dwarfs with their short term H- α variability and to understand rotation-activity relations in M dwarfs. Such programs shall be explored in future using medium resolution spectroscopy mode ($\delta\lambda \sim 2000$) of MFOSC-P.

7 ACKNOWLEDGMENTS

MFOSC-P instrument is being funded by the Department of Space, Government of India through Physical Research Laboratory. MKS thanks to the Director, PRL for supporting MFOSC-P development program. The research leading to these results has received funding from the French "Programme National de Physique Stellaire" and the Programme National de Planetologie of CNRS (INSU). The computations were performed at the *Pôle Scientifique de Modélisation Numérique* (PSMN) at the *École Normale Supérieure* (ENS) in Lyon, and at the *Gesellschaft für Wissenschaftliche Datenverarbeitung Göttingen* in collaboration with the Institut für Astrophysik Göttingen. DH was supported by the Collaborative Research Centre SFB 881 "The Milky Way System" (subproject A4) of the German Research Foundation (DFG). This work has made use of data from the European Space Agency (ESA) mission *Gaia* (<https://www.cosmos.esa.int/gaia>), processed by the *Gaia* Data

Processing and Analysis Consortium (DPAC, <https://www.cosmos.esa.int/web/gaia/dpac/consortium>). Funding for the DPAC has been provided by national institutions, in particular the institutions participating in the *Gaia* Multilateral Agreement. This research has made use of the VizieR catalogue access tool, CDS, Strasbourg, France (DOI : 10.26093/cds/vizieR). The authors thank anonymous referee for his/her useful suggestions to improve the manuscript.

REFERENCES

- Allard F., Hauschildt P. H., 1995, *ApJ*, **445**, 433
Allard F., Hauschildt P. H., Schwenke D., 2000, *ApJ*, **540**, 1005
Allard F., Guillot T., Ludwig H.-G., Hauschildt P. H., Schweitzer A., Alexander D. R., Ferguson J. W., 2003, in E. Martín ed., IAU Symposium Vol. 211, Brown Dwarfs. pp 325–+
Allard F., Homeier D., Freytag B., 2010, preprint, ([arXiv:1011.5405](https://arxiv.org/abs/1011.5405))
Allard F., Homeier D., Freytag B., 2011, in Johns-Krull C., Browning M. K., West A. A., eds, Astronomical Society of the Pacific Conference Series Vol. 448, Astronomical Society of the Pacific Conference Series. p. 91 ([arXiv:1011.5405](https://arxiv.org/abs/1011.5405))
Allard F., Homeier D., Freytag B., Sharp C. M., 2012, in Reylé C., Charbonnel C., Schultheis M., eds, EAS Publications Series Vol. 57, EAS Publications Series. pp 3–43 ([arXiv:1206.1021](https://arxiv.org/abs/1206.1021)), [doi:10.1051/eas/1257001](https://doi.org/10.1051/eas/1257001)
Allard F., Homeier D., Freytag B., Schaffenberger W., Rajpurohit A. S., 2013, *Memorie della Societa Astronomica Italiana Supplementi*, **24**, 128
Andersen J., et al., 1995, *The Messenger*, **79**, 12
Barber R. J., Tennyson J., 2008, in European Planetary Science Congress 2008. p. 870
Barber R. J., Tennyson J., Harris G. J., Tolchenov R. N., 2006, *MNRAS*, **368**, 1087
Bochanski J. J., West A. A., Hawley S. L., Covey K. R., 2007, *AJ*, **133**, 531
Buzzoni B., et al., 1984, *The Messenger*, **38**, 9
Caffau E., Maiorca E., Bonifacio P., Faraggiana R., Steffen M., Ludwig H.-G., Kamp I., Busso M., 2009, *A&A*, **498**, 877
Caffau E., Ludwig H.-G., Steffen M., Freytag B., Bonifacio P., 2011, *Sol. Phys.*, **268**, 255
Chabrier G., 2003, *ApJ*, **586**, L133
Chakraborty A., et al., 2014, *PASP*, **126**, 133
Chakraborty A., Roy A., Sharma R., Mahadevan S., Chaturvedi P., Prasad N. J. S. S. V., Anandarao B. G., 2018a, *AJ*, **156**, 3
Chakraborty A., Thapa N., Kumar K., Neelam P. J. S. S. V., Sharma R., Roy A., 2018b, in *Proc. SPIE*. p. 107026G, [doi:10.1117/12.2313055](https://doi.org/10.1117/12.2313055)
Frith J., et al., 2013, *MNRAS*, **435**, 2161
Gizis J. E., 1997, *AJ*, **113**, 806
Gizis J. E., Reid I. N., Hawley S. L., 2002, *AJ*, **123**, 3356
Hawley S. L., Gizis J. E., Reid I. N., 1996, *AJ*, **112**, 2799
Henry T. J., Walkowicz L. M., Barto T. C., Golimowski D. A., 2002, *AJ*, **123**, 2002
Kirkpatrick J. D., Henry T. J., McCarthy Jr. D. W., 1991, *ApJS*, **77**, 417
Kirkpatrick J. D., Henry T. J., Simons D. A., 1995, *AJ*, **109**, 797
Lépine S., Gaidos E., 2011, *AJ*, **142**, 138
Lépine S., Shara M. M., Rich R. M., 2003, *AJ*, **126**, 921
Lépine S., Rich R. M., Shara M. M., 2007, *ApJ*, **669**, 1235
Lépine S., Hilton E. J., Mann A. W., Wilde M., Rojas-Ayala B., Cruz K. L., Gaidos E., 2013, *AJ*, **145**, 102
Luri X., et al., 2018, *A&A*, **616**, A9
Martín E. L., Delfosse X., Basri G., Goldman B., Forveille T., Zapatero Osorio M. R., 1999, *AJ*, **118**, 2466
Ochsenbein F., Bauer P., Marcout J., 2000, *A&AS*, **143**, 23

- Passegger V. M., Wende-von Berg S., Reiners A., 2016, *A&A*, **587**, [A19](#)
- Passegger V. M., et al., 2019, arXiv e-prints, p. [arXiv:1907.00807](#)
- Plez B., 1998, *A&A*, **337**, [495](#)
- Rajpurohit A. S., et al., 2012, *A&A*, **545**, [A85](#)
- Rajpurohit A. S., Reylé C., Allard F., Homeier D., Schultheis M., Bessell M. S., Robin A. C., 2013, *A&A*, **556**, [A15](#)
- Rajpurohit A. S., Reylé C., Allard F., Scholz R.-D., Homeier D., Schultheis M., Bayo A., 2014, *A&A*, **564**, [A90](#)
- Rajpurohit A. S., Reylé C., Allard F., Homeier D., Bayo A., Mousis O., Rajpurohit S., Fernández-Trincado J. G., 2016, *A&A*, **596**, [A33](#)
- Rajpurohit A. S., Allard F., Teixeira G. D. C., Homeier D., Rajpurohit S., Mousis O., 2018a, *A&A*, **610**, [A19](#)
- Rajpurohit A. S., Allard F., Rajpurohit S., Sharma R., Teixeira G. D. C., Mousis O., Kamlesh R., 2018b, *A&A*, **620**, [A180](#)
- Reid I. N., Hawley S. L., Gizis J. E., 1995, *AJ*, **110**, [1838](#)
- Reiners A., Basri G., 2008, *ApJ*, **684**, [1390](#)
- Scholz R. D., Meusinger H., Jahreiß H., 2005, *A&A*, **442**, [211](#)
- Skrutskie M. F., et al., 2006, *AJ*, **131**, [1163](#)
- Srivastava M. K., Jangra M., Dixit V., Munjal B. S., Arora H., Mavani T., 2018, in Proc. SPIE. p. 107024I, [doi:10.1117/12.2309306](#)
- Wright E. L., et al., 2010, *AJ*, **140**, [1868](#)
- York D. G., et al., 2000, *AJ*, **120**, [1579](#)